Molecular Therapy
Oncolytics
Original Article

Therapeutic potential of IBP as an autophagy inducer for treating lung cancer via blocking PAK1/Akt/mTOR signaling

Huimin Bu,[1,2,4] Shirui Tan,[3,4] Bo Yuan,[1] Xiaomei Huang,[1] Jiebang Jiang,[1] Yejiao Wu,[1] Jihong Jiang,[1] and Rongpeng Li[1]

[1]Key Laboratory of Biotechnology for Medicinal Plants of Jiangsu Province and School of Life Sciences, Jiangsu Normal University, Xuzhou, Jiangsu 221116, PR China; [2]Department of Physiology, Xuzhou Medical University, Xuzhou, Jiangsu 221004, PR China; [3]Center of Life Sciences, School of Life Sciences, Yunnan University, Kunming, Yunnan 650500, PR China

Lung cancer is the most frequent and fatal malignancy in humans worldwide, yet novel successful drugs for control of this disease are still lacking. *Ipomoea batatas* polysaccharides (IBPs) have been implicated in inhibiting diverse cancer types, but their functions in mitigating lung cancer are largely unknown. In this study, we identify a role of IBP in inhibiting lung cancer proliferation. We found that IBP significantly impedes the proliferation of lung cancer cells by inducing cytostatic macroautophagy both *in vitro* and *in vivo*. Mechanistically, IBP specifically promotes ubiquitination-mediated degradation of PAK1 (p21-activated kinase 1) and blocks its downstream Akt1/mTOR signaling pathway, leading to increased autophagic flux. In lung cancer xenografts in mice, IBP-induced cytostatic autophagy suppresses tumor development. Through site-directed mutational analysis, the underlying signaling augments ubiquitination via PAK1-ubiquitin interaction. Collectively, this work unravels the molecular mechanism underpinning IBP-induced cytostatic autophagy in lung cancer and characterizes IBP as a potential therapeutic agent for lung cancer treatment.

INTRODUCTION

Leading to 1.8 million deaths per year all over the world, lung cancer is the most frequent and fatal malignancy in humans.[1] To date, the best therapeutic strategy for lung cancer is complete surgical resection, which offers a 40%, 5-year survival rate, on average, for patients.[2] However, at the time of diagnosis, over 75% of lung cancer patients present are unsuitable for surgery due to their advanced or metastatic diseases.[3,4]

In the last decades, multiple novel therapy strategies for lung cancers have been introduced, including platinum-based double chemotherapy, antiangiogenic agents, targeted therapy, and immunotherapy.[5,6] Although having improved lung cancer from a disease with an extremely poor prognosis to a more treatable one, the current therapeutic strategies remain, more or less, flawed. For example, the chimeric antigen receptor T cell (CAR-T) immunotherapy, used for non-small cell lung cancer, easily causes an uncontrolled "cytokine storm," which activates severe inflammation responses, acute respiratory distress syndrome, and even multiple organ failure.[7] Chemotherapeutic drugs are another type of commonly used medicine for lung cancers; however, there are significant defects for these drugs, such as nonspecific distribution in the body; excessive toxicities to healthy cells; as well as less severe symptoms of uneasiness, nausea, and fatigue.[8] Thus, there is still an urgent need for effective therapeutic agents for lung cancers.

Autophagy is a conserved eukaryotic stress-response pathway in which cells sequester damaged or surplus proteins and organelles in double-membrane vesicles and deliver them to lysosomes for degradation.[9] The classic trigger of autophagy is nutrient shortage, but recent studies determined that autophagy plays seminal roles in other cellular functions, such as antimicrobial host defense and tumor development,[10] acting as a double-edged sword in tumorigenesis and metastasis. On the one hand, autophagy could protect cancer cells from chemotherapy- or radiation-induced stresses by eliminating the source of cellular damage.[11] For example, microRNA (miR)-1251-5p was proven to enhance tumor growth through upregulation of LC3B.[12] The release of the high-mobility group box 1 protein (HMGB1) in conditioned medium from dying cells by chemotherapeutic drugs and resistant cells triggered autophagy for chemoresistance and regrowth in the surviving cancer cells.[13] The vascular endothelial growth factor C/Polyclonal antibody to neuropilin 2 (VEGF-C/NRP-2) axis is involved in the activation of autophagy, which helps cancer cell survival following

Received 9 October 2020; accepted 29 October 2020;
https://doi.org/10.1016/j.omto.2020.10.014.

[4]These authors contributed equally

Correspondence: Rongpeng Li, Key Laboratory of Biotechnology for Medicinal Plants of Jiangsu Province and School of Life Sciences, Jiangsu Normal University, Xuzhou, Jiangsu 221116, PR China.
E-mail: lirongpeng@jsnu.edu.cn
Correspondence: Jihong Jiang, Key Laboratory of Biotechnology for Medicinal Plants of Jiangsu Province and School of Life Sciences, Jiangsu Normal University, Xuzhou, Jiangsu 221116, PR China.
E-mail: jhjiang@jsnu.edu.cn

treatment.[14] On the contrary, other studies revealed the anticancer properties of autophagy. Allelic loss of the essential autophagy gene *beclin1*, as well as autophagy-related gene 4 (*atg4*), results in a quicker tumorigenesis.[15,16] Ivermectin induced cytostatic autophagy and thus, inhibited the proliferation of breast cancer cells.[17] A new cardenolide-3′-epi-12β-hydroxyfroside (HyFs) treatment in lung cancers was investigated and shown to inhibit cell proliferation by inducing autophagy.[18] These studies collectively suggest that autophagy is a potential therapeutic target for anticancer therapy, and understanding the mechanism of autophagy and the regulatory signaling pathway involved in cancer cells is important before its clinical use.

For centuries, *Ipomoea batatas* has been a well-known food supplement used in traditional Chinese medicine in many Asian countries, promoting human health and longevity. *I. batatas* polysaccharides (IBP) corresponds to a major active ingredients derived from this plant, having diverse effects, such as anti-oxidant,[19] anti-inflammatory,[20,21] and anticancer functions.[22] Wu et al.[23] reported that IBP possessed *in vitro* antioxidant (scavenging 1,1-Diphenyl-2-picrylhydrazyl radical 2,2-Diphenyl-1-(2,4,6-trinitrophenyl)hydrazyl (DPPH) radicals: 1,1-diphenyl-2-picrylhydrazyl; 2,2-diphenyl-1-(2,4,6-trinitrophenyl) hydrazyl; and α,α-diphenyl-β-picrylhydrazyl, chelating ferrous ions and reducing power) and antitumor (against gastric cancer cells SGC7901 and SW620) activities in a dose-dependent manner. IBPs also have a marked effect on inhibitory tumors on the nasopharyngeal carcinoma cell S18 and hepatic cancer cell H22-bearing mice.[24] Recently, IBP was identified to be a promising anticancer agent. The mixture therapy group of low-dose IBP inhibited tumor proliferation, with obvious protective effects on the thymus and spleen weight atrophy resulting from 5-fluorouracil (5-FU) and antagonism of the decrease in white cell counts.[25] However, the inner molecular mechanisms underlying IBP-mediated suppression of tumor growth remain poorly understood.

In this study, we identified IBP as anti-inhibitor of lung cancer proliferation by stimulating autophagy both *in vivo* and *in vitro*. Mechanistically, IBP promotes ubiquitination-mediated degradation of PAK1, blocks the Akt/mammalian target of rapamycin (mTOR) signaling pathway, and then activates autophagy in lung cancer cells. Our data suggest that IBP-induced autophagy is a primary role for inhibiting lung cancer growth and that IBP may be a cogent drug therapeutic approach for lung cancer treatment.

RESULTS

IBP inhibits the growth of lung cancer cells

To investigate the anticancer effect of IBP in lung cancer cells, we used a 3-(4,5-dimethylthiazol-2-yl)-2,5-diphenyltetrazolium bromide (MTT) assay to test the growth of three human lung cancer cell lines (A549, H460, and H1299) and one murine lung epithelial cell line (MLE-12, used as normal cell control) following IBP treatment. As shown in Figure 1A, IBP remarkably inhibited the cell viability of lung cancer cells in a dose-dependent manner. The addition of 40 μg/mL IBP completely suppressed the growth of lung cancer cells in 48 h, whereas 50% MLE-12 cells remained alive (Figure 1A). The 5-Ethynyl 2'-deoxyuridine (EdU) proliferation assay showed that the percentage of EdU-incorporating live cells was significant in IBP-treated cells compared to the controls (Figure 1B). By the same token, IBP markedly suppressed the proliferation of A549 and H460 cells, which was determined by reduced clonogenic survival (Figure 1C). To examine whether the cell death induced by IBP is apoptosis, we quantified the apoptotic lung cancer cells by TUNEL staining and flow cytometry assay. We found that IBP treatment did not increase the apoptosis in A549 and H460 cells (Figures 1D and S1A), suggesting that IBP-induced suppression of cancer cell proliferation was independent of apoptosis.

We then investigated the anticancer effect of IBP on lung cancer *in vivo*. We employed an implanted subcutaneous lung cancer model by, respectively, injecting A549 and H460 cells into BALB/c mice and then treating with IBP. Data showed that xenografts in IBP-treated mice grew more slowly than control mice treated with placebo (Figures 1E, 1F, S1B, and S1C). Macroscopically, the tumor weight of IBP-treated mice was significantly lower than that of control mice (Figures 1E and S1B). Consistently, tumor size was reduced in IBP-treated mice compared to that of the control group (Figures 1G and S1D). In general, a high dose of IBP (10 mg/kg) treatment has a better efficiency of inhibiting tumors than a low dose (1 mg/kg) treatment (Figures 1E–1G and S1B–S1D). To clarify the role of IBP in proliferation inhibition, xenografts were stained for Ki67, a marker widely used to assess the proliferative fraction in cancers. Xenografts of IBP-treated mice showed much slighter Ki67 staining than that of control mice (Figures 1H and S1E). These findings collectively reveal that IBP inhibits the growth of lung cancer both *in vitro* and *in vivo*.

IBP possesses decent anticancer cell proliferation by stimulating autophagy

Recent studies demonstrated that drug-induced autophagy plays critical roles in anticancer therapies; thus, we proposed that IBP may also inhibit lung cancer growth by inducing autophagy.[18] We first investigated the formation of the autophagosome membrane in IBP-treated A549 and H460 cells by testing the conversion of LC3-I to lipidated LC3-II and the distribution of endogenous LC3 puncta. In IBP-treated cells, we determined a significant increase of LC3-II conversion (Figures 2A and S2A) by an immunoblotting assay and an increased LC3 puncta accumulation under confocal microscope observation (Figure 2B). Cells were also stained with acridine orange (AO) to detect the formation of acidic vesicular organelles (AVOs), which are associated with the establishment of an autophagic process.[26] Cytoplasmic AVO formation was quickly observed in IBP-treated cells compared to that of control cells (Figure 2C). We then checked the formation of double-membraned autophagosomes in mouse xenografts and A549 cells by transmission electronic microscopy observation. As shown in Figures 2D and S2B, numerous autophagic vacuoles containing lamellar structures or residual digested material and empty vacuoles were observed in the IBP-treated group but not in that of the placebo group, suggesting that IBP not only increased the number of vacuoles but also increased the number of mature autophagosomes. Furthermore, immunohistochemistry (IHC) data showed that IBP-treated tumor cells displayed stronger LC3-II straining than that in control mouse (Figure 2E). Coincidentally, IBP-treated xenografts had a similar

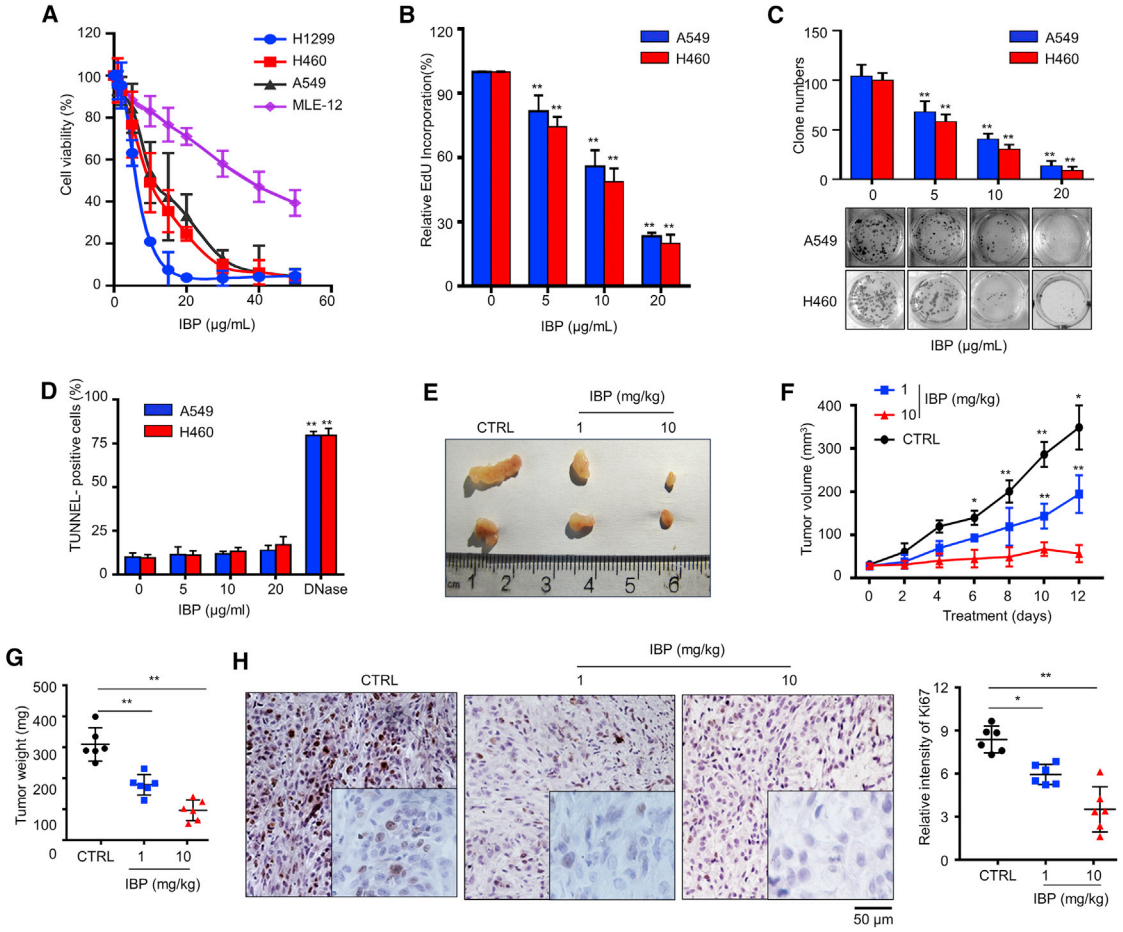

Figure 1. IBP inhibits the growth of lung cancer cells

(A) A549, H460, H1299, and MLE-12 cells were incubated in the presence of IBP at different concentrations (0, 1, 2, 5, 10, 15, 20, 30, 40, and 50 μg/mL) for 48 h. Cell viability was assessed by MTT assay at a wavelength of 570 nm. (B) A549 and H460 cells were incubated in the presence of IBP in the indicated concentrations for 48 h. Cell viability was assessed by EdU incorporation assays. (C) A549 and H460 were cultured in the indicated concentrations of IBP for 14 days. Cell clone number was counted. (D) A549 and H460 cells were treated with IBP as (C), and apoptotic cells were assessed by TUNEL staining. (E–G) 3×10^7 of A549 cells per mouse was subcutaneously inoculated in the back of BALB/c mice. 1 or 10 mg/kg of IBP was administered by intraperitoneal injection every 2 days. Mice were sacrificed on day 12, and tumors were excised, photographed, and weighted. (H) Ki67 expression in tumor xenografts was examined by IHC. Representative images were provided as indicated; scale bar, 50 μm. Data are mean ± SD from three independent experiments. One-way ANOVA (Tukey's post hoc); *$p < 0.05$; **$p < 0.01$.

tendency in LC3-II conversion (Figure 2F). These data suggest that IBP activates autophagy in lung cancer cells both *in vitro* and *in vivo*.

Beclin1 and Atg5 are two autophagy-related proteins critical for autophagosome formation. IBP activated the expression of both Beclin1 and Atg5 (Figures 2A, S2C, and S2D), suggesting that IBP promotes autophagosome formation. To search after the mechanism by which IBP activates autophagy, we investigated if IBP could induce autophagosome by regulating the interaction of Beclin1 with positive regulators Atg14 and Vps34 and with the negative regulator Bcl-2.[27] As shown in Figure 3A, IBP treatment increased the binding of Beclin1 with Atg14L and Vps34, respectively. On the contrary, cells treated with IBP reduced the binding of Beclin1 with Bcl-2 (Figure 3B), suggesting that IBP can enhance autophagy by increasing the interaction of Beclin1/Atg14L/Vps34 and decreasing the interaction of Beclin1/Bcl-2. To corroborate the evidence for formation of autophagosomes induced by IBP, we transfected a tandem monomeric RFP-GFP-LC3 (red fluorecent protein-green fluorecent protein-LC3) plasmid into A549 and H460 cells. As shown in Figures 3C–3F, IBP increased formation of autophagosomes and autolysosome, which were indicated by yellow fluorescence and red fluorescence. These results determine that IBP induces autophagy in lung cancer cells.

SQSTM1 (sequestosome 1), an indicator of autophagic flux, is a selective autophagic substrate that interacts with LC3 and ubiquitin and a cargo receptor for autophagic degradation of ubiquitinated targets.[28] Immunoblotting data showed that SQSTM1 was reduced by IBP in A549 and H460 (Figures 2A and S2E), suggesting that IBP promotes

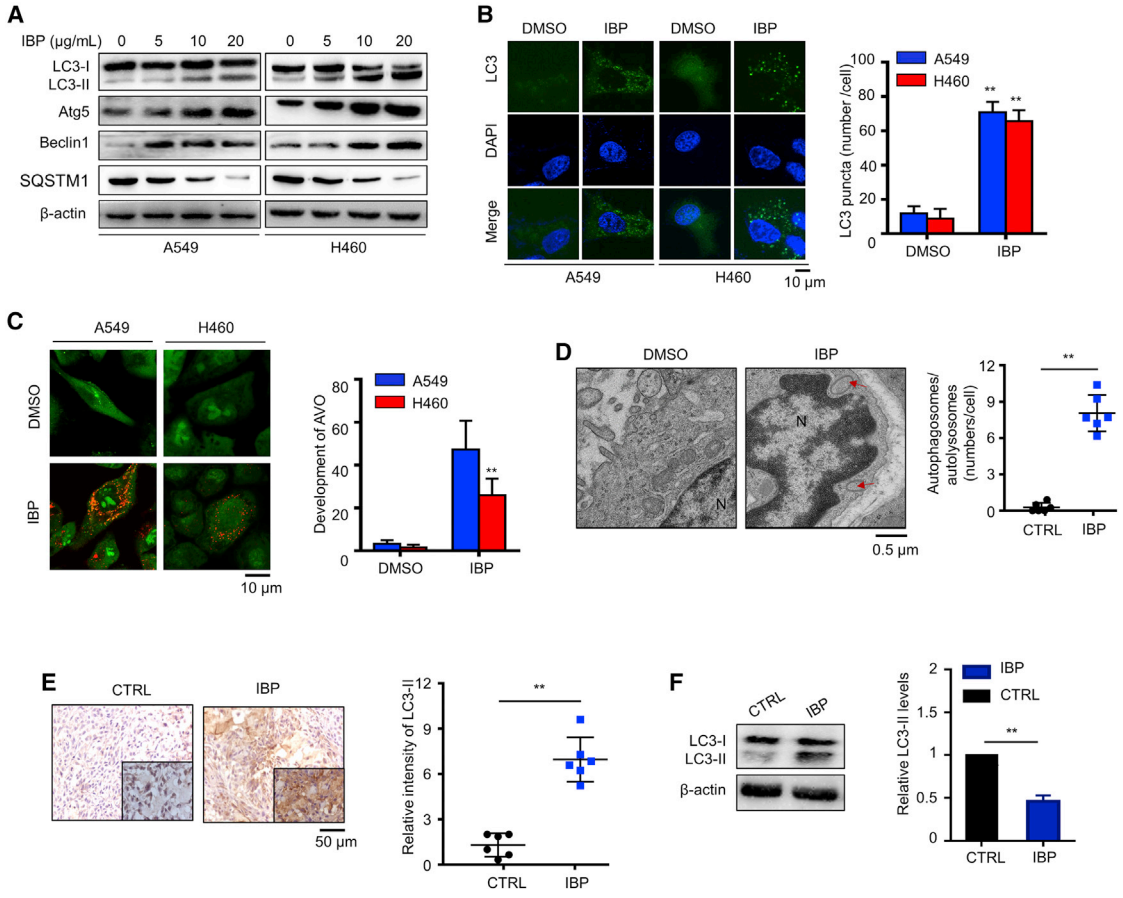

Figure 2. IBP induces autophagy in lung cancer cells

(A) LC3, Atg5, Beclin1, and SQSTM1 expression in A549 and H460 were measured by immunoblotting. Cells were treated with the indicated concentrations of IBP for 48 h. (B) A549 and H460 cells were transfected with LC3-GFP for 24 h and then were treated with 10 μg/mL IBP for another 48 h. Formation of endogenous LC3 puncta in cells was detected by confocal laser-scanning microscopy (CLSM). Scale bar, 10 μm. (C) Autophagy measured by acridine orange staining of cells treated as in (B). Orange puncta were acidic vesicular organelles (AVOs). Scale bar, 10 um. (D) Autophagy measured by transmission electron microscopy in xenografts. Arrows, autophagosomes. Scale bar, 0.5 um. (E) *In situ* analysis of LC3 abundance (brown) in xenograft tissues by IHC. Nuclei were counterstained by hematoxylin (blue). Scale bar, 50 μm. (F) The level of LC3-II in xenografts tissue was assessed by immunoblotting. Data are mean ± SD from three independent experiments. One-way ANOVA (Tukey's post hoc); *p < 0.05; **p < 0.01.

autophagy flux in lung cancer cells. A549 and H460 were pretreated with an autophagy inhibitor 3-methyladenine (3-MA)[29] and then were transfected with a tandem monomeric RFP-GFP-LC3. IBP increased the formation of autophagosomes and autolysosome, and combinatorial treatment of 3-MA and IBP led to less accumulation of autophagosomes (Figures 3C–3F). These data determined that IBP induces autophagic flux in lung cancer cells.

To investigate whether autophagy was relevant in the anticancer effect of IBP, A549 and H460 cells were, respectively, transfected with Atg5 or Beclin1 small interfering RNA (siRNA) to block cell autophagy. After IBP treatment, cell viability was, respectively, determined by MTT and colony-formation analysis. Data showed that knockdown of either Beclin1 or Atg5 markedly restored cell growth in IBP-treated cells (Figures 4A and 4B). In addition, we obtained similar results in cells combinatorial treated with IBP and 3-MA or another autophagy early-stage inhibitor LY294002, which inhibits the formation of the Beclin1-phosphatidylinositol 3-kinase (PI3K) complex to inactivate autophagy (Figure 4C).[30] These data suggested that IBP-inhibited lung cancer cell growth was dependent on autophagy.

IBP induced autophagy via the PI3K/Akt/mTOR signaling pathway

Recent studies have reported that the Akt/mTOR pathway negatively regulates autophagy in tumorigenesis.[31] Therefore, we hypothesized that the Akt/mTOR signaling pathway is also involved in IBP-induced autophagy in lung cancer cells. We first demonstrated that IBP repressed phosphorylation of Akt (p-Akt), p-mTOR, and 4EBP1 in both A549 and H460 cells, which were obtained by an immunoblotting assay (Figures 4D and S2F–S2H).

In addition, we transfected the CA-Akt plasmid (a constitutively active form of Akt) into lung cancer cells to recover IBP-induced Akt/mTOR inhibition (Figures 4E and S3A).[32] Immunoblotting assay

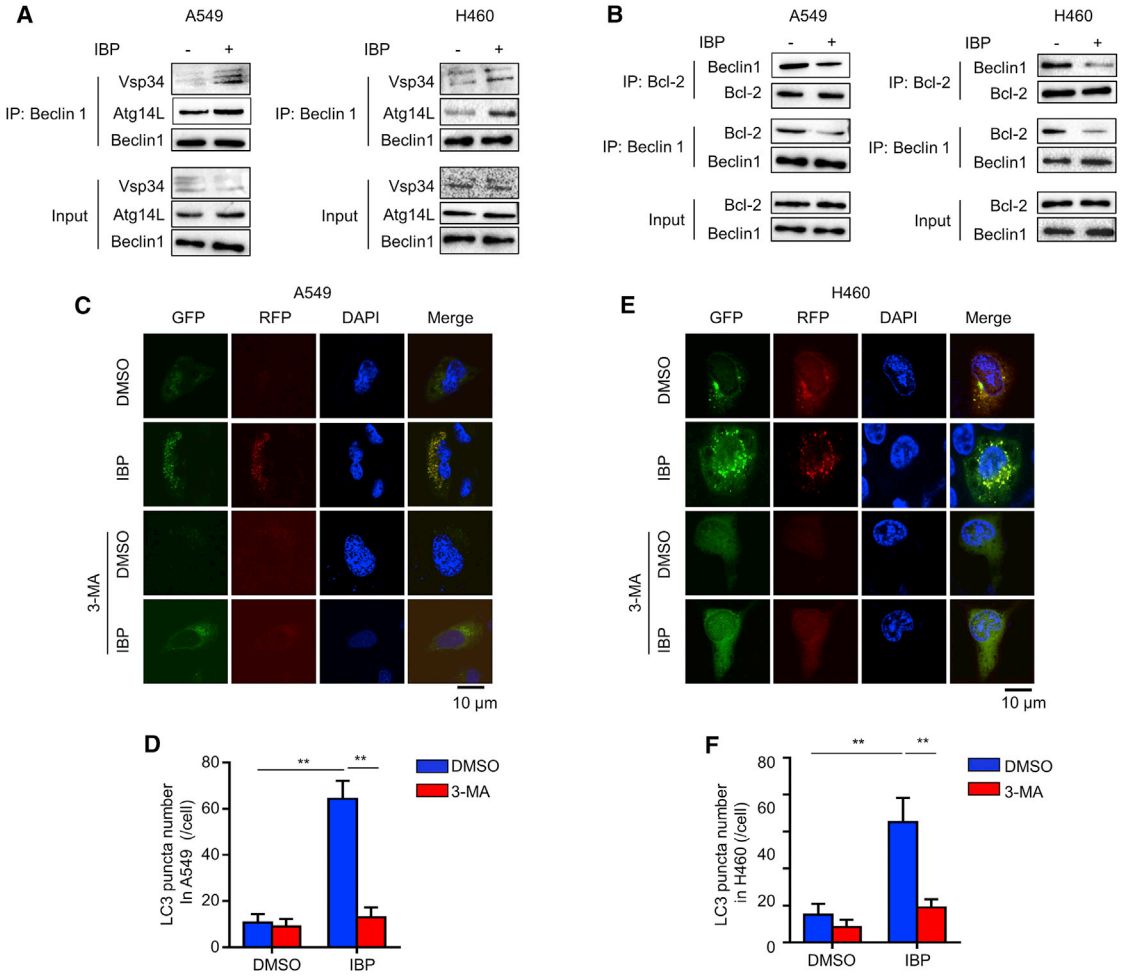

Figure 3. IBP promotes autophagy flux in lung cancer cells

(A) A549 and H460 cells were treated with 10 μg/mL IBP for 48 h. The interaction among Beclin1, Atg14L, and Vps34 in indicated cells was determined by coimmunoprecipitation assay. (B) Interaction between Beclin1 and Bcl-2 in A549 and H460 cells was tested as in (A). (C–F) A549 and H460 cells were transfected with RFP-GFP tandem fluorescent-tagged LC3 (RFP-GFP-LC3) for 24 h, and then cells were treated with 10 μg/mL IBP alone or in combination with 10 μM 3-MA for 48 h. Formation of endogenous LC3 puncta in cells was detected by CLSM. Scale bars, 10 μm. Data are mean ± SD from three independent experiments. One-way ANOVA (Tukey's post hoc); *$p < 0.05$; **$p < 0.01$.

and confocal microscopy observation determined that Akt activation significantly reduced LC3-II conversion and LC3 puncta accumulation in IBP-treated A549 cells (Figures 4E, 4F, and S3B). These data collectively indicated that IBP induces autophagy in lung cancer cells through the Akt/mTOR signaling pathway.

IBP induced autophagy through a PAK1/Akt1/mTOR axis in lung cancer cells

As is reported, PAK1 is abnormally expressed in diverse tumors and is associated with cancer cell proliferation and invasiveness.[33] In breast cancer cells, PAK1 is involved in ivermectin-induced autophagy by promoting the p-Akt to regulate the Akt/mTOR signaling pathway.[17] We proposed that a similar mechanism exists in lung cancer cells. Our data showed that IBP treatment decreased PAK1 expression in a dose-dependent manner, both in A549 and H460 cells (Figure 5A). To test the regulation of PAK1 on the Akt/mTOR signaling pathway, we, respectively, transfected PAK1 siRNA and PAK1-hemagglutinin (HA) plasmid into A549 cells to knock down or overexpress PAK1. In PAK1 knockdown cells, we observed a significantly decreased p-Akt, whereas in PAK1 overexpressing cell, enforced PAK1 expression promoted p-Akt (Figures S3C and S3D). Coimmunoprecipitation (coIP) data indicated a direct interaction of PAK1 and Akt in A549 cells (Figure S3E). In addition, IBP reduced this interaction (Figure S3E), suggesting that IBP interferes with the interaction between PAK1 and Akt1, thus regulating Akt/mTOR signaling in lung cancer cells.

To determine the effect of PAK1 in IBP-induced autophagy, we further assessed LC3 puncta in PAK1 knockdown cells and PAK1 overexpressing cells, respectively, with or without IBP treatment. Compared to that in A549 control cells, PAK1 knockdown resulted in LC3 puncta accumulation, but IBP treatment did not accelerate LC3 puncta accumulation in PAK1-interfered A549 cells (Figure 5B).

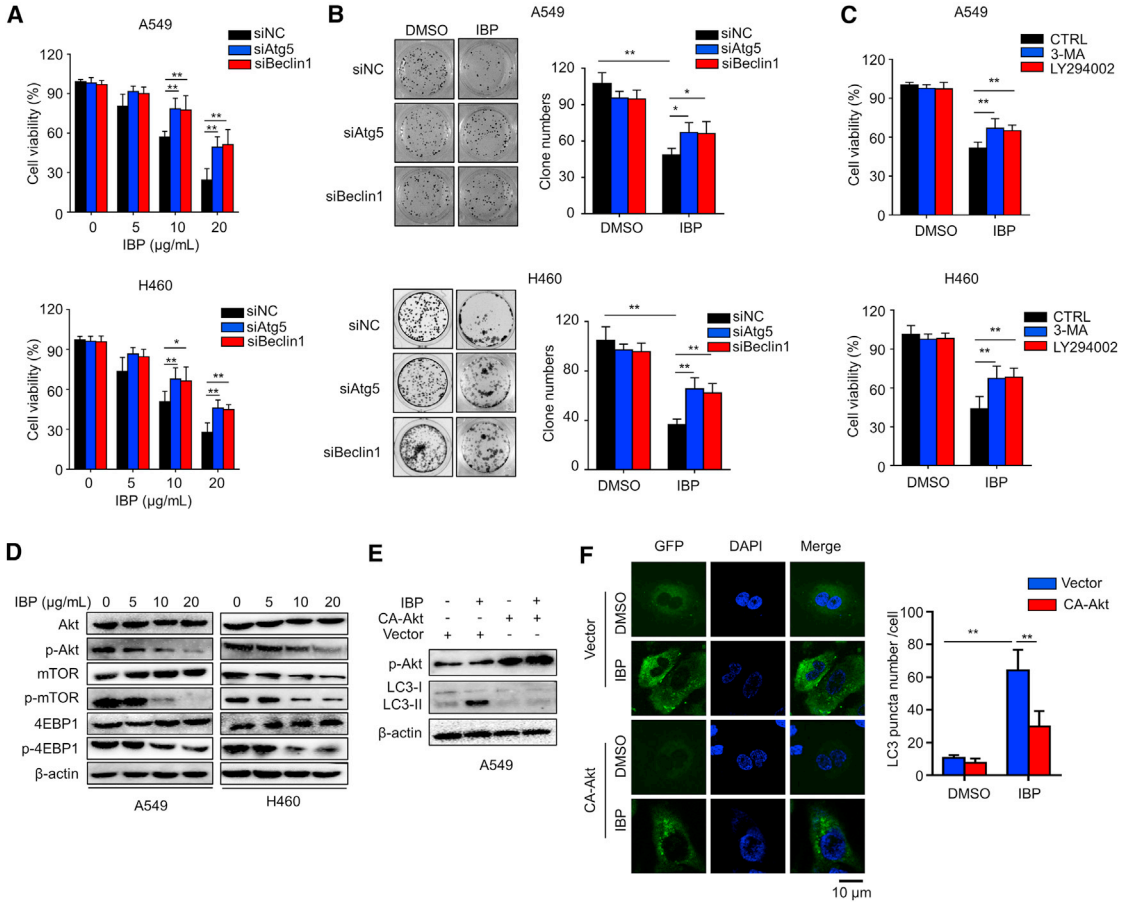

Figure 4. Inhibition of autophagy represses the antiproliferative effect of IBP in lung cancer cells

(A) Cells were transfected with 50 nM siRNA against Atg5 or Beclin1 for 48 h and then treated with 10 μg/mL IBP for another 48 h. Cell viability was detected by MTT assay. (B) Cell clone number was counted. (C) Cells were treated with 3-MA or LY294002 in the presence or absence of IBP (10 μg/mL) for 48 h, and then the proliferation rate was measured by MTT assay. (D) A549 and H460 cells were treated with IBP at different concentrations (0, 5, 10, and 20 μg/mL) for 48 h and then lysed and applied to detect phosphorylation of Akt (p-Akt; S473), p-mTOR (S2448), p-p70S6K (S424/T421), and p-4EBP1 (S65/T70) by immunoblotting. Total Akt, mTOR, and 4EBP1 expression was used as the internal control (Ctrl), respectively. (E) A549 cells were transfected with a constitutively active Akt (CA-Akt) for 24 h and were then treated with 10 μg/mL IBP for another 48 h. Cell lysates were collected and performed for immunoblotting of p-Akt and LC3 lipidation. (F) A549 cells were cotransfected with GFP-RFP-LC3 and CA-Akt or vector for 24 h, and then cells were treated with 10 μg/mL IBP for another 48 h. LC3 puncta were detected by CLSM. Scale bar, 10 um. Data are mean ± SD from three independent experiments. One-way ANOVA (Tukey's post hoc); *$p < 0.05$; **$p < 0.01$.

In contract, PAK1 overexpression repressed IBP-induced LC3 puncta (Figure 5C). Consistently, immunoblotting analysis showed increased levels of PAK1 and p-Akt1 and p-mTOR in xenografts from IBP-treated mice compared to the solvent control group (Figure 5D). In addition, the control group showed more p-Akt and p-PAK1 staining than that in the IBP-treated group (Figure 5E). These data collectively determined the PAK1/Akt/mTOR axis as a key signaling pathway of IBP-induced autophagy in lung cancer cells.

IBP stimulates autophagy in lung cancer cells by ubiquitination-mediated PAK1 degradation

To determine the inner mechanism involved, we performed reverse-transcriptase polymerase chain reaction (RT-PCR) to quantify the mRNA level of PAK1 and found that IBP treatment had no apparent effect on PAK1 mRNA expression in both A549 and H460 cells (Figure 6A). This result revealed that IBP did not decrease PAK1 expression by inhibiting its mRNA transcription. To investigate whether PAK1 was degraded through the proteasome/ubiquitination pathway, we, respectively or in combination, treated cells with IBP and a proteasome inhibitor MG132 and then measured the PAK1 expressing levels by an immunoblotting assay. Data showed that the protein level of PAK1 was only downregulated by IBP treatment alone, and MG132 stabilized PAK1 in A549 and H460 cells (Figure 6B), suggesting that PAK1 may be degraded through the proteasome/ubiquitination pathway.

We then simultaneously transfected PAK1-HA and Flag-tagged ubiquitin (Flag-Ub) plasmids into A549 cells and then measured the protein levels of PAK1 to determine whether IBP-induced PAK1

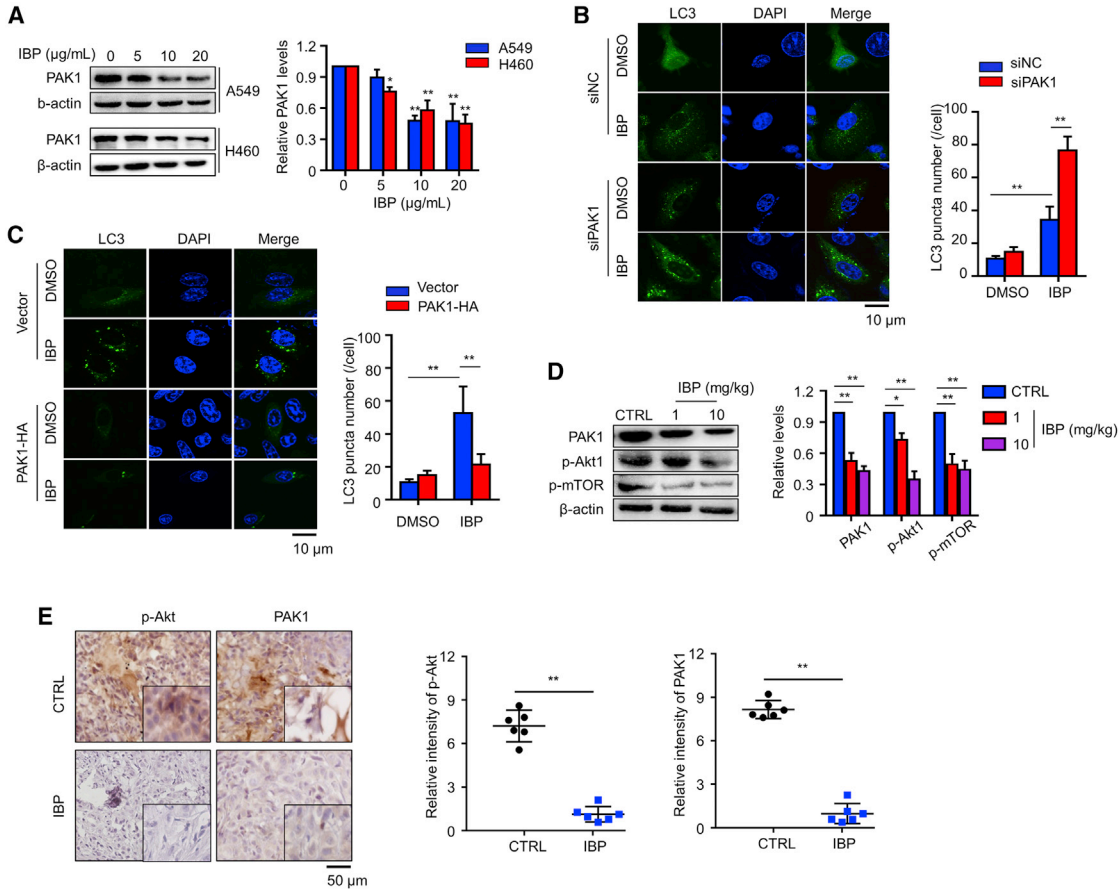

Figure 5. IBP induces autophagy through downregulation of PAK1 in lung cancer cells

(A) Cells treated with the indicated concentrations of IBP (0, 5, 10, and 20 μg/mL) for 48 h. PAK1 expressions in A549 and H460 cells were measured by immunoblotting. (B) A549 cells were cotransfected with GFP-RFP-LC3 and Ctrl or PAK1 siRNA for 48 h and then were treated with 10 μg/mL IBP for another 48 h. CLSM was employed to determine LC3 puncta. Scale bar, 10 um. (C) A549 cells were cotransfected with GFP-RFP-LC3 and HA-PAK1 for 24 h, and then cells were treated as in (B). LC3 puncta were detected by CLSM. Scale bar, 10 um. (D) The expression of PAK1, p-Akt, and p-mTOR in xenograft tissues was assessed by immunoblotting. (E) *In situ* analysis of p-Akt and PAK1 abundance (brown) in xenograft tissues by IHC. Nuclei were counterstained by hematoxylin (blue). Scale bar, 50 μm. Data are mean ± SD from 3 independent experiments. One-way ANOVA (Tukey's post hoc); *$p < 0.05$; **$p < 0.01$.

reduction is dependent on proteasome-mediated degradation. As shown in Figure 6C, IBP significantly induced PAK1-Ub conjugation, and it was further strengthened by proteasome inhibitor MG132 treatment. Lysine residues (K11, K29, K39, and K148) of PAK1 were reported as potential ubiquitination sites of PAK1 in breast cancer cells.[17] To test whether these lysine residues were also critical in lung cancer cells, we constructed lysine mutants of PAK1 using two mutation strategies. For one strategy, six indicated lysine residues were, respectively, mutated to arginine (K11R, K29R, K39R, K148R, K162R, and K256R). Immunoblotting analysis showed that the ubiquitination of these mutants was similar as the wild type (Figure 6D). For another mutation strategy, we constructed another six mutants (K11, K29, K39, K148, K162, and K256), and each contained a single candidate lysine (for example, K256 had one lysine at position 256 with the other five arginines instead of lysines). Ubiquitin was efficiently conjugated with PAK1 mutants containing K11, K29, K39, K148, or K162 (Figure 6E). These results revealed that in lung cancer cells, IBP also downregulates PAK1 by targeting the lysine residues at K11, K29, K39, K148, or K162 and promoting the ubiquitin/proteasome-mediated degradation, a similar role of PAK1 in breast cancer cells.

DISCUSSION

Natural products derived from medicinal plants, such as cardenolides, flavonoids, and terpenes, have received considerable attention in recent years due to their diverse pharmacological properties, especially anticancer activities.[18,34] Our lab has previously isolated a polysaccharide (IBP) from sweet potato *I. batatas* that suppressed B16 and HepG2 tumor growth. In this study, we characterized the detailed mechanisms underlying the growth-inhibitory effect of IBP in anti-lung cancer (Figure 6F). First, IBP treatment remarkably inhibits cell growth in lung cancer A549, H460, and H1299 cell lines and

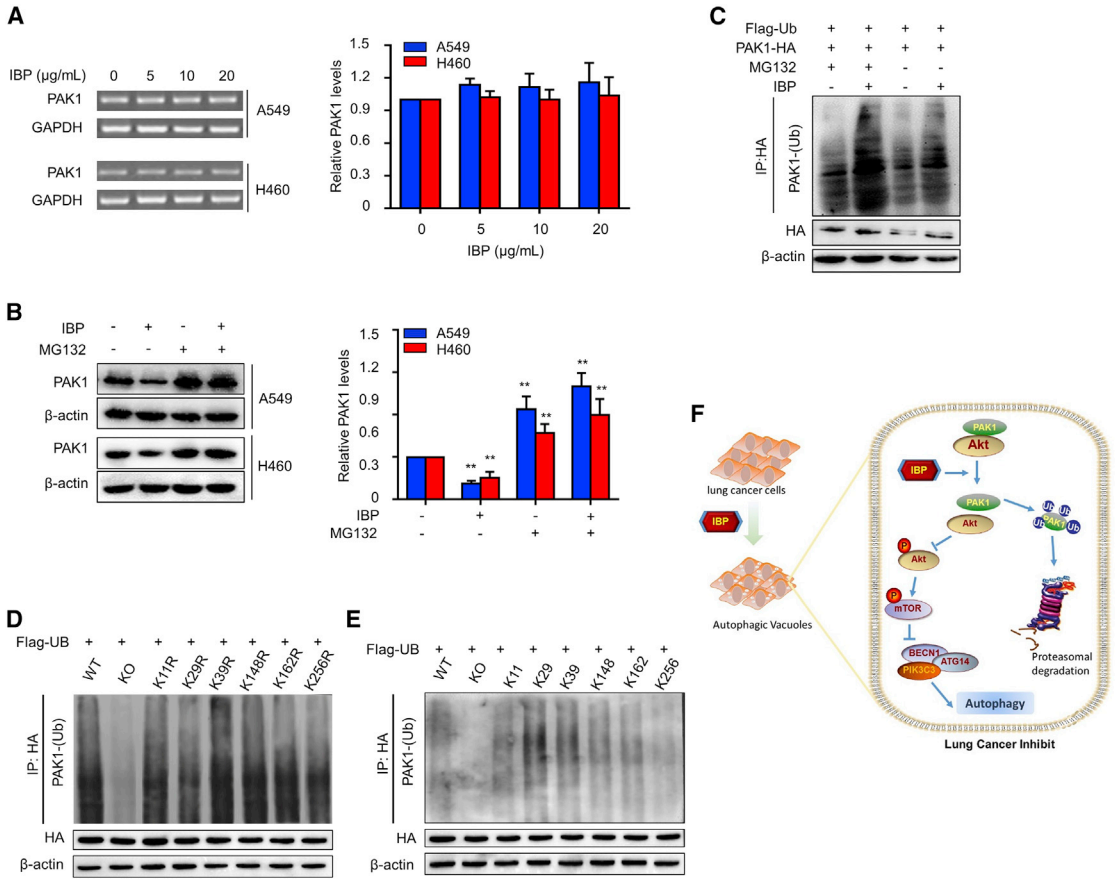

Figure 6. IBP promotes ubiquitin degradation of PAK1

(A) A549 cells were treated with the indicated concentrations of IBP (0, 5, 10, and 20 μg/mL) for 48 h. PAK1 mRNA expression was evaluated by RT-PCR. (B) Cells were treated with 10 μg/mL IBP alone or combine treated with 10 mM MG132 for 48 h. Protein levels of PAK1 in A549 and H460 were determined by immunoblotting. (C) A549 cells were cotransfected with Flag-ubiquitin (Ub) and PAK1-HA plasmids for 24 h and then were treated as in (B). (D and E) A549 cells were cotransfected with Flag-Ub, and PAK1-HA plasmids contained one lysine mutant (D) and five mutations (E). Interaction between HA and PAK1-Ub in indicated A549 cells (C–E) was determined by coimmunoprecipitation assay. (F) Proposed model for the role of IBP in regulating the autophagy in lung cancer cells. WT, wild type; KO, knockout. Data are a representation of 3 independent experiments. One-way ANOVA (Tukey's post hoc); *p < 0.05; **p < 0.01.

repressed xenograft growth in a mouse lung cancer model (Figure 1). Second, IBP activates cytostatic autophagy in lung cancer cells by suppressing the Akt/mTOR signaling pathway, leading to the inhibition of tumor growth (Figure 4). Third, IBP-induced autophagy in lung cancer cells is associated with decreased PAK1 via the ubiquitination-mediated degradation pathway (Figures 5 and 6).

Studies have indicated that many anticancer agents can induce autophagy in cancer cells,[17,18] but the potential prospect of autophagy in cancer therapy is still elusive. Our studies support the idea that autophagy is not only a consequence protector of chemotherapy or radiotherapy but also has an inhibitory effect on cancer cells.[30] To date, four different types of autophagy have been recognized as being involved in anticancer treatment, including cytoprotective, nonprotective, cytotoxic, and cytostatic autophagy.[35] Cytoprotective autophagy plays a prosurvival role in cancer cells by removing damage organelles and recycling nutrients upon anticancer treatment.[36] In contrast, cytotoxic autophagy results in autophagic cell death or promotes apoptosis,[37] whereas cytostatic autophagy inhibits cell growth in an apoptosis-independent way.[38] In this study, we confirmed that IBP-induced autophagy inhibited the proliferation of lung cancer cells in an apoptosis-independent way (Figures 1D and S1A). In addition, no significant apoptosis was observed even in IBP-treated lung cancer cells when IBP-mediated autophagy was interrupted by siRNA against Atg5 or Beclin1 (Figures S4A and S4B), further suggesting that IBP treatment induces cytostatic autophagy, which is not related to apoptosis in lung cancer cells. Similar findings have been investigated in other cancer types.[39] For example, Dou et al.[17] reported that ivermectin-induced cytostatic autophagy inhibits the proliferation of breast cancer cells. In lung cancer cell inhibition, Sun et al.[18] found that a cardenolide HyFS induces autophagy in a cytoprotective manner. Here, we produced the first evidence that autophagy induced by IBP could inhibit lung cancer cells in a cytostatic way.

The Akt/mTOR signaling is a critical pathway for autophagy activation and regulation of cell proliferation in diverse types of cancers, including breast cancer, bladder cancer, prostate cancer, and lung cancer.[40] In this study, our data showed that the Akt/mTOR signaling pathway was significantly inhibited by IBP in both A549 and H460 cells, again proving evidence of the function of Akt/mTOR in lung cancer.[41] Several factors, including PI3K, heat shock protein (HSP)90, PAK1, phosphate and tension homology deleted on chromsome ten (PTEN), etc., were reported to regulate the p-Akt and its downstream signaling,[17,18,42,43] but it is unclear which factor is critical in the IBP-regulated Akt/mTOR axis. Our data showed that IBP obviously decreased the expression of PAK1, but it did not change the protein levels of HSP90 and PTEN (Figure S4C). These results figured out the PAK1/Akt/mTOR axis is a specific signaling pathway in IBP-induced autophagy. As reported, ivermectin downregulated PAK1 protein levels by promoting the ubiquitin-mediated degradation in breast cancer cells. Here, our results also showed that PAK1 and its client protein Akt protein levels were downregulated by ubiquitin-mediated degradation of PAK1 in IBP-treated cells. This result suggested that IBP may be a potent agent in the induction of PAK1-Ub, and increased PAK1-Ub might be a general switch to induce autophagy in cancer types. Moreover, we showed that IBP promoted ubiquitin-mediated degradation of PAK1 by targeting the residues at K11, K29, K39 K148, or K162 in lung cancer cells, which is similar to the ivermectin mechanism in breast cancer cells.[17] In conclusion, the PAK1-Ub and PAK1/Akt/mTOR signaling pathway maybe worth exploration as a therapeutic strategy for many types of cancer treatment.

In summary, this study, for the first time, demonstrated that IBP is a potential agent against lung cancer growth by inducing PAK1/Akt/mTOR-mediated cytostatic autophagy. However, although here, we have emphatically confirmed the role of IBP in cytostatic autophagy, the accurate target protein of IBP remains unknown. Our further study may focus on investigating the target protein of IBP and validating the effect of IBP in conjunction with IBP to activate cytostatic autophagy. Four candidate cell membrane proteins were selected for our future work, since these proteins could recognize polysaccharides and path signals into inner cells, including Toll-like receptor (TLR)2, TLR4, Dectin-1, and EGFR.[44–46] As reported, homogeneous polysaccharide from *Phoma herbarum* interacted with TLR2, TLR4, and Dectin-1 to stimulate B cell differentiation.[47] Polysaccharides extracted from *Dictyophora indusiata* could activate macrophages through binding to Dectin-1.[46] Another potential IBP-targeted protein is epidermal growth factor receptor (EGFR), because polysaccharide from *Sepiella maindroni* ink was able to bind to EGFR and thus suppressed the cancer cell migration, invasion, and expression.[44] The understanding of the molecular mechanism underlying IBP anticancer activity will evaluate the clinical therapeutic application of IBP for treatment of lung cancer.

MATERIALS AND METHODS

Mice

Male BALB/c mice (6 to 8 weeks) were obtained from Xipuer-BiKai Experimental Animals (Shanghai, PR China). All of the animal studies were approved by the Institutional Animal Care and Treatment Committee of Xuzhou Medical University. The animal experimental procedures, including treatment, care, and endpoint choice, followed the "Animal Research: Reporting of *In Vivo* Experiments" guidelines. Animal experiments were performed with randomization. For the lung cancer mouse model, 1×10^6 A549 and H460 lung cancer cells were suspended in 0.05 M phosphate-buffered saline (PBS) and subcutaneously injected into BALB/c mice. When the tumor volume reached at $\sim$50 mm^3, mice were randomly divided into three groups and intraperitoneally injected with vehicle (DMSO; Wak-Chemie) and IBP (1 mg/kg or 10 mg/kg) every 2 days, respectively. Mice were euthanized for analysis after 12 days. Tumor tissues were isolated and frozen in liquid nitrogen or fixed in 10% formalin immediately.

Cell culture

Human lung cancer cell lines A549, H460, H1299, and MLE-12 were purchased from Shanghai Cell Bank of the Chinese Academy of Sciences (Shanghai, PR China). According to the ATCC guidelines, A549, H460, and H1299 cells were maintained in RPMI-1640 medium, and MLE-12 cells were maintained in DMEM/F12 medium, supplemented with 10% fetal bovine serum (FBS; PAN-Biotech), 100 U/mL penicillin (Thermo Fisher Scientific), and 100 U/mL streptomycin (Thermo Fisher Scientific) in a humidified incubator at 37°C under 5% CO_2 atmosphere.

Assays for cell viability

The short-term effects of IBP on lung cancer cell growth were determined through the MTT (Sigma-Aldrich) assay, as previously described.[48] EdU incorporation assays were performed to examine cell proliferation after treatment with IBP. A549 and H460 were incubated in 100 μM with Edu (RiboBio, Guangzhou, China) for 2 h. Then, cell proliferation was detected as previously described.[49] EdU-positive cell was calculated as (EdU add-in cells/Hoechst-stained cells) × 100%.

The long-term effects of IBP on lung cancer cell proliferation were measured with a colony-formation assay. Generally, cells were seeded at a density of 300 cells/well in 24-well plates and treated with the indicated concentration of IBP or vehicle control. The medium was changed every 2 days. After 14 days, the colonies were stained with Giemsa (Sigma-Aldrich) for 15 min and washed with PBS three times. The visible colonies were captured by the Molecular Imager Gel System (Bio-Rad) and counted using ImageJ software (National Institutes of Health).

Apoptosis analysis by flow cytometer and TUNEL staining

Apoptosis was detected by the Annexin V-fluorescein isothiocyanate (FITC)/propidium iodide (PI) apoptosis Detection Kit (RiboBio, Guangzhou, China), according to the manufacturer's protocol. A549 and H460 were labeled and detected with a flow cytometer. The percentage of cells negative for stains (viable cells), positive for Annexin-V (apoptotic cells), and positive for PI (dead cells) was acquired.

The TUNEL staining method was also used to detect apoptosis. After lung cancer cells were treated with IBP, the staining was performed,

according to the manufacturer's protocol. The fluorescence was measured by fluorescence microscopy. The assay was repeated 3 times.

AO staining

AO staining was employed to evaluate autophagy. AO (Sigma-Aldrich) was dissolved in PBS containing 5% FBS (10 μM). A549 and H460 were treated with or without IBP at certain concentrations for 48 h and then incubated with AO at 37°C for 5 min. Cells were washed three times by PBS and then observed by confocal microscope.[50]

Plasmids

The human PAK1 (GenBank: NM_001128620.1) coding region with C-terminal HA tag was amplified by PCR and cloned into the *Bam*HI and *Eco*RI sites of the pcDNA3.1 vector (#13031; Addgene). Constructed plasmids that were ported into DH5α transformants were selected and maintained in Luria-Bertani (LB) medium containing 100 μM ampicillin (Sigma-Aldrich). The PCR primers for the PAK1 full sequence were as follows: sense primer: 5′-cgcggatccatgtc aaataacggcctagac-3′; anti-sense primer: 5′-ccggaattcgctgcagcaatcagtgg ag-3′. CA-Akt (myrAkt delta4-129) and Flag-Ub were kindly provided by Dr. Canhua Huang (Sichuan University, PR China).

Transfection of siRNA, plasmids, and inhibitors

Beclin1, Atg5, PAK1, and scrambled siRNA were obtained from Santa Cruz Biotechnology (Santa Cruz, CA, USA). A549 cells were transfected with siRNA (5 nM), LC3-GFP (100 ng), and pcDNA3.1 plasmids (100 ng) using Exfect2000 (Vazyme Biotech), according to the manufacturer's instruction. In some cases, A549 cells were treated with a 10-nM autophagy inhibitor (3-MA and LY294002) for 4 h, as indicated, respectively.[51] 3-MA was obtained from Solarbio. LY294002 was purchased from Beyotime Biotechnology.

Transmission electron microscopy

Transmission electron microscopy was performed to identify autophagosomes.[26] Briefly, the tumor tissue was fixed in the following steps: (1) in a fixative solution for 2 h at 4°C, (2) in 4% ice-cold glutaraldehyde overnight, and (3) in 2% osmium tetroxide and dehydrated in a series of graded ethanol solutions. Samples were rinsed in propylene oxide and impregnated with epoxy resins. Ultrathin sections (60 nm thickness) were prepared by a Sorvall MT5000 microtome (Dupont Instruments) after dehydration and then stained with 2% lead citrate and 0.4% uranyl acetate. Samples were observed by transmission electron microscopy (FEI Tecnai G2), and the autophagic vacuoles in the cytoplasmic area were calculated using Image-Pro Plus version 3 software (Media Cybernetics).

LC3 puncta observation

A549 and H460 cells were transfected with LC3-RFP-GFP plasmids or LC3-GFP plasmids using Exfect2000 (Vazyme Biotech) for 24 h, according to the manufacturer's instruction. Cells were treated with indicated concentrations of IBP for 24 h and then observed under a LSM 510 Meta Confocal Microscope (Carl Zeiss Micro Imaging). LC3 puncta values were derived from 100 cells/sample.[51]

RT-PCR array

Total RNA was extracted using TRIzol (Invitrogen), followed by DNase I digestion. A total of 1 μg RNA was used for cDNA synthesis, using RT and random hexamers from the RevertAid First Strand cDNA Synthesis Kit (Thermo Fisher Scientific). The PAK1 primers are the following primers: 5′-ATGGATGAAGGCCAAATTGCA-3′ and 5′-GGTTCAGAAAGTCCCGGAAGATAG-3′. PCR was performed in a DNA thermal cycler (Maxygen), according to a standard protocol as follows: 1 cycle of 95°C for 5 min; 35 cycles of 95°C for 30 s, annealing of 56°C for 30 s, and 72°C for 1 min; a final extension at 72°C for 10 min; and holding at 4°C. The PCR products (5 μL) were analyzed by electrophoresis through 1% agarose gels and visualized by SYBR Gold staining. Results were normalized to the expression of human glyceraldehyde-3-phosphate dehydrogenase (GAPDH).

IHC

IHC analysis was performed, as previously described.[48] Tumor tissues from three independent mice were fixed in 10% formalin (Sigma-Aldrich) for 24 h and then embedded in paraffin using a routine histologic procedure, and 4-μm sections were cut. After dewaxing, rehydration, and antigen retrieval, tumor sections were blocked with 3% bovine serum albumin (BSA; Thermo Fisher Scientific) for 3 h and incubated overnight with primary antibodies (Abs; Ki67, PAK1, p-Akt1, LC3-II). Ki67, PAK1, p-Akt1, and LC3-II in tumor tissues were detected using the EXPOSE mouse and rabbit specific horseradish peroxidase (HRP)/3,3'-diaminobenzidine (DAB) Detection IHC kit (Abcam) and observed by DM5000B microscopy (Leica). The immunostaining intensity (A) was indicated by four grades (0, negative; 1, weakly positive; 3, positive; and 4, strongly positive), and the proportion of staining-positive cells (B) was divided into five grades (0, <5%; 1, 6%–25%; 2, 26%–50%; 3, 51%–75%; 4, 76%–100%). The final score was calculated as A × B.

Immunoblotting

Rabbit monoclonal Abs against p-Akt (#4060), total forms of Akt (#2938), p-mTOR (#5536), mTOR (#2972), p-4EBP1 (#9451), 4E-BP1 (#9452), PAK1 (#2602), HA tag (#3714), Atg14 (#96752), Vps34 (#4263), PI3K (#4249), LC3A/B (#4108), Beclin1 (#3495), and Atg5 (#12994) were purchased from Cell Signaling Technology. Mouse monoclonal Abs against ubiquitin (sc-271289) were purchased from Santa Cruz Biotechnology.

The samples derived from cells and tumor homogenates were lysed in Mammalian Protein Extraction Reagent (Thermo Fisher Scientific), separated by electrophoresis on 12% SDS-polyacrylamide gel electrophoresis and transferred to nitrocellulose transfer membranes (Merck Millipore, Cork, Ireland). Proteins were detected using primary Abs at a concentration of 1:1,000 (Cell Signaling Technology) and were incubated overnight. Specific interaction with the primary Abs was detected using corresponding secondary Abs conjugated to HRP (Biosharp), and signals were developed using the enhanced

chemiluminescence (ECL) reagents (Biosharp). Gel bands were quantified by ImageJ software, and data are presented as mean ± SD from three independent immunoblotting assays.[51] Phosphorylated and total protein levels were determined and quantified by three successive immunoblotting membranes.

CoIP

To obtain whole-cell lysates, indicated A549 cells were homogenized in lysis buffer containing phosphatase inhibitor (1:10,000) and protease inhibitor cocktail (1:100; SWBIO). Then total cell lysates were mixed with the indicated immunoprecipitation Ab, which was coupled to agarose beads (A/G, 50:50; MedChemExpress). Immunoprecipitates were washed 3 times with RIPA ((Radio Immunoprecipitation Assay)) buffer, separated by SDS-polyacrylamide gel electrophoresis, and transferred to nitrocellulose membranes. Proteins were detected using the detective Abs and were incubated overnight. Labeling of the first Abs was incubated with relevant secondary Abs conjugated to HRP and detected using ECL reagents.[48]

Statistical analysis

Experiments were performed in triplicate and repeated at least three independent times. Data were shown as mean ± SD. Statistical differences were evaluated by one-way ANOVA (Tukey's post hoc test) for multiple comparisons or by two-tailed Student's t test for two experimental group comparisons using GraphPad Prism 7 software. Differences were accepted as significant at $p < 0.05$.[51]

SUPPLEMENTAL INFORMATION

Supplemental Information can be found online at https://doi.org/10.1016/j.omto.2020.10.014.

ACKNOWLEDGMENTS

We sincerely thank Dr. Canhua Huang and Dr. Kui Wang (Sichuan University, China) for kindly providing CA-Akt and Flag-Ub vectors. The experiments in this article were partly completed in the Public Experimental Research Center of Xuzhou Medical University. We thank Dr. Meng Wang and Qingli Huang for their enthusiastic help in the experiment of transmission electron microscopy and Fuxing Dong for his enthusiastic help in the experiment of laser-scanning confocal microscopy. This work was supported by the Project of the Natural Science Foundation of the Jiangsu Higher Education Institutions of China (18KJA18003), Xuzhou Applied and Basic Research (KC18009), National Natural Science Foundation of China (NSFC81703569, 81870005), Priority Academic Program Development of Jiangsu Higher Education Institutions (PAPD), and Program of Jiangsu Province (KYCX18-2123).

AUTHOR CONTRIBUTIONS

R.L. and J.J. (Jihong Jiang) conceived and designed the research. H.B. and S.T. performed most of the experiments. B.Y., X.H., J.J. (Jiebang Jiang), and Y.W. isolated and purified IBP. H.B. and R.L. wrote the manuscript. J.J. reviewed and revised the manuscript.

DECLARATION OF INTERESTS

The authors declare no competing interests.

REFERENCES

1. Bray, F., Ferlay, J., Soerjomataram, I., Siegel, R.L., Torre, L.A., and Jemal, A. (2018). Global cancer statistics 2018: GLOBOCAN estimates of incidence and mortality worldwide for 36 cancers in 185 countries. CA Cancer J. Clin. *68*, 394–424.
2. Miller, K.D., Nogueira, L., Mariotto, A.B., Rowland, J.H., Yabroff, K.R., Alfano, C.M., Jemal, A., Kramer, J.L., and Siegel, R.L. (2019). Cancer treatment and survivorship statistics, 2019. CA Cancer J. Clin. *69*, 363–385.
3. Siegel, R.L., Miller, K.D., and Jemal, A. (2018). Cancer statistics, 2018. CA Cancer J. Clin. *68*, 7–30.
4. Chen, W., Sun, K., Zheng, R., Zeng, H., Zhang, S., Xia, C., Yang, Z., Li, H., Zou, X., and He, J. (2018). Cancer incidence and mortality in China, 2014. Chin. J. Cancer Res. *30*, 1–12.
5. Ernani, V., Steuer, C.E., and Jahanzeb, M. (2017). The End of Nihilism: Systemic Therapy of Advanced Non-Small Cell Lung Cancer. Annu. Rev. Med. *68*, 153–168.
6. Sun, Y., Dai, H., Chen, S., Zhang, Y., Wu, T., Cao, X., Zhao, G., Xu, A., Wang, J., and Wu, L. (2018). Disruption of Chromosomal Architecture of cox2 Locus Sensitizes Lung Cancer Cells to Radiotherapy. Mol. Ther. *26*, 2456–2465.
7. Wang, L., Yao, R., Zhang, L., Fan, C., Ma, L., and Liu, J. (2019). Chimeric antigen receptor T cell therapy and other therapeutics for malignancies: Combination and opportunity. Int. Immunopharmacol. *70*, 498–503.
8. Siegel, R.L., Jemal, A., Wender, R.C., Gansler, T., Ma, J., and Brawley, O.W. (2018). An assessment of progress in cancer control. CA Cancer J. Clin. *68*, 329–339.
9. Marx, V. (2015). Autophagy: eat thyself, sustain thyself. Nat. Methods *12*, 1121–1125.
10. Levine, B. (2007). Cell biology: autophagy and cancer. Nature *446*, 745–747.
11. Liu, Y., Tang, J., Liu, D., Zhang, L., He, Y., Li, J., Gao, L., Tang, D., Jin, X., and Kong, D. (2018). Increased autophagy in EOC re-ascites cells can inhibit cell death and promote drug resistance. Cell Death Dis. *9*, 419.
12. Shao, Y., Liu, X., Meng, J., Zhang, X., Ma, Z., and Yang, G. (2019). MicroRNA-1251-5p Promotes Carcinogenesis and Autophagy via Targeting the Tumor Suppressor TBCC in Ovarian Cancer Cells. Mol. Ther. *27*, 1653–1664.
13. Huang, C.Y., Chiang, S.F., Chen, W.T., Ke, T.W., Chen, T.W., You, Y.S., Lin, C.Y., Chao, K.S.C., and Huang, C.Y. (2018). HMGB1 promotes ERK-mediated mitochondrial Drp1 phosphorylation for chemoresistance through RAGE in colorectal cancer. Cell Death Dis. *9*, 1004.
14. Wang, J., Huang, Y., Zhang, J., Xing, B., Xuan, W., Wang, H., Huang, H., Yang, J., and Tang, J. (2018). NRP-2 in tumor lymphangiogenesis and lymphatic metastasis. Cancer Lett. *418*, 176–184.
15. Santana-Codina, N., Mancias, J.D., and Kimmelman, A.C. (2017). The Role of Autophagy in Cancer. Annu. Rev. Cancer Biol. *1*, 19–39.
16. Mariño, G., Salvador-Montoliu, N., Fueyo, A., Knecht, E., Mizushima, N., and López-Otín, C. (2007). Tissue-specific autophagy alterations and increased tumorigenesis in mice deficient in Atg4C/autophagin-3. J. Biol. Chem. *282*, 18573–18583.
17. Dou, Q., Chen, H.N., Wang, K., Yuan, K., Lei, Y., Li, K., Lan, J., Chen, Y., Huang, Z., Xie, N., et al. (2016). Ivermectin Induces Cytostatic Autophagy by Blocking the PAK1/Akt Axis in Breast Cancer. Cancer Res. *76*, 4457–4469.
18. Sun, Y., Huang, Y.H., Huang, F.Y., Mei, W.L., Liu, Q., Wang, C.C., Lin, Y.Y., Huang, C., Li, Y.N., Dai, H.F., and Tan, G.H. (2018). 3′-epi-12β-hydroxyfroside, a new cardenolide, induces cytoprotective autophagy via blocking the Hsp90/Akt/mTOR axis in lung cancer cells. Theranostics *8*, 2044–2060.
19. Zhai, X., Zhu, C., Li, Y., Zhang, Y., Duan, Z., and Yang, X. (2018). Optimization for pectinase-assisted extraction of polysaccharides from pomegranate peel with chemical composition and antioxidant activity. Int. J. Biol. Macromol. *109*, 244–253.
20. Wold, C.W., Kjeldsen, C., Corthay, A., Rise, F., Christensen, B.E., Duus, J.O., and Inngjerdingen, K.T. (2018). Structural characterization of bioactive heteropolysaccharides from the medicinal fungus Inonotus obliquus (Chaga). Carbohydr. Polym. *185*, 27–40.

21. Zhao, G., Kan, J., Li, Z., and Chen, Z. (2005). Characterization and immunostimulatory activity of an (1–>6)-a-D-glucan from the root of Ipomoea batatas. Int. Immunopharmacol. *5*, 1436–1445.

22. Belhaj, D., Athmouni, K., Ahmed, M.B., Aoiadni, N., El Feki, A., Zhou, J.L., and Ayadi, H. (2018). Polysaccharides from Phormidium versicolor (NCC466) protecting HepG2 human hepatocellular carcinoma cells and rat liver tissues from cadmium toxicity: Evidence from in vitro and in vivo tests. Int. J. Biol. Macromol. *113*, 813–820.

23. Wu, Q., Qu, H., Jia, J., Kuang, C., Wen, Y., Yan, H., and Gui, Z. (2015). Characterization, antioxidant and antitumor activities of polysaccharides from purple sweet potato. Carbohydr. Polym. *132*, 31–40.

24. Khan, T., Date, A., Chawda, H., and Patel, K. (2019). Polysaccharides as potential anticancer agents-A review of their progress. Carbohydr. Polym. *210*, 412–428.

25. Yu, J., Ji, H., and Liu, A. (2018). Preliminary Structural Characteristics of Polysaccharides from Pomelo Peels and Their Antitumor Mechanism on S180 Tumor-Bearing Mice. Polymers (Basel) *10*, E419.

26. Thomé, M.P., Filippi-Chiela, E.C., Villodre, E.S., Migliavaca, C.B., Onzi, G.R., Felipe, K.B., and Lenz, G. (2016). Ratiometric analysis of Acridine Orange staining in the study of acidic organelles and autophagy. J. Cell Sci. *129*, 4622–4632.

27. Sun, Y., Yao, X., Zhang, Q.J., Zhu, M., Liu, Z.P., Ci, B., Xie, Y., Carlson, D., Rothermel, B.A., Sun, Y., et al. (2018). Beclin-1-Dependent Autophagy Protects the Heart During Sepsis. Circulation *138*, 2247–2262.

28. Jain, A., Rusten, T.E., Katheder, N., Elvenes, J., Bruun, J.A., Sjøttem, E., Lamark, T., and Johansen, T. (2015). p62/Sequestosome-1, Autophagy-related Gene 8, and Autophagy in Drosophila Are Regulated by Nuclear Factor Erythroid 2-related Factor 2 (NRF2), Independent of Transcription Factor TFEB. J. Biol. Chem. *290*, 14945–14962.

29. Mizushima, N., Yoshimori, T., and Levine, B. (2010). Methods in mammalian autophagy research. Cell *140*, 313–326.

30. Kocaturk, N.M., Akkoc, Y., Kig, C., Bayraktar, O., Gozuacik, D., and Kutlu, O. (2019). Autophagy as a molecular target for cancer treatment. Eur. J. Pharm. Sci. *134*, 116–137.

31. Moore, J., Megaly, M., MacNeil, A.J., Klentrou, P., and Tsiani, E. (2016). Rosemary extract reduces Akt/mTOR/p70S6K activation and inhibits proliferation and survival of A549 human lung cancer cells. Biomed. Pharmacother. *83*, 725–732.

32. Bodine, S.C., Stitt, T.N., Gonzalez, M., Kline, W.O., Stover, G.L., Bauerlein, R., Zlotchenko, E., Scrimgeour, A., Lawrence, J.C., Glass, D.J., and Yancopoulos, G.D. (2001). Akt/mTOR pathway is a crucial regulator of skeletal muscle hypertrophy and can prevent muscle atrophy in vivo. Nat. Cell Biol. *3*, 1014–1019.

33. Higuchi, M., Onishi, K., Kikuchi, C., and Gotoh, Y. (2008). Scaffolding function of PAK in the PDK1-Akt pathway. Nat. Cell Biol. *10*, 1356–1364.

34. Mann, C.D., Neal, C.P., Garcea, G., Manson, M.M., Dennison, A.R., and Berry, D.P. (2009). Phytochemicals as potential chemopreventive and chemotherapeutic agents in hepatocarcinogenesis. Eur. J. Cancer Prev. *18*, 13–25.

35. Gewirtz, D.A. (2014). The four faces of autophagy: implications for cancer therapy. Cancer Res. *74*, 647–651.

36. McAlpine, F., Williamson, L.E., Tooze, S.A., and Chan, E.Y. (2013). Regulation of nutrient-sensitive autophagy by uncoordinated 51-like kinases 1 and 2. Autophagy *9*, 361–373.

37. Pal, S., Salunke-Gawalib, S., and Konkimallaa, V.B. (2017). Induction of Autophagic Cell Death in Apoptosis-resistant Pancreatic Cancer Cells using Benzo[α]phenoxazines Derivatives, 10-methyl-benzo[α]phenoxazine-5-one and benzo[α]phenoxazine-5-one. Anticancer. Agents Med. Chem. *17*, 115–125.

38. Jiang, S., Zhao, Y., Zhang, T., Lan, J., Yang, J., Yuan, L., Zhang, Q., Pan, K., and Zhang, K. (2018). Galantamine inhibits β-amyloid-induced cytostatic autophagy in PC12 cells through decreasing ROS production. Cell Prolif. *51*, e12427.

39. Chang, C.H., Bijian, K., Wernic, D., Su, J., da Silva, S.D., Yu, H., Qiu, D., Asslan, M., and Alaoui-Jamali, M.A. (2019). A novel orally available seleno-purine molecule suppresses triple-negative breast cancer cell proliferation and progression to metastasis by inducing cytostatic autophagy. Autophagy *15*, 1376–1390.

40. Nitulescu, G.M., Van De Venter, M., Nitulescu, G., Ungurianu, A., Juzenas, P., Peng, Q., Olaru, O.T., Grădinaru, D., Tsatsakis, A., Tsoukalas, D., et al. (2018). The Akt pathway in oncology therapy and beyond (Review). Int. J. Oncol. *53*, 2319–2331.

41. Chen, Q.Y., Jiao, D.M., Wu, Y.Q., Chen, J., Wang, J., Tang, X.L., Mou, H., Hu, H.Z., Song, J., Yan, J., et al. (2016). MiR-206 inhibits HGF-induced epithelial-mesenchymal transition and angiogenesis in non-small cell lung cancer via c-Met /PI3k/Akt/mTOR pathway. Oncotarget *7*, 18247–18261.

42. Li, Y.C., He, S.M., He, Z.X., Li, M., Yang, Y., Pang, J.X., Zhang, X., Chow, K., Zhou, Q., Duan, W., et al. (2014). Plumbagin induces apoptotic and autophagic cell death through inhibition of the PI3K/Akt/mTOR pathway in human non-small cell lung cancer cells. Cancer Lett. *344*, 239–259.

43. Mundi, P.S., Sachdev, J., McCourt, C., and Kalinsky, K. (2016). AKT in cancer: new molecular insights and advances in drug development. Br. J. Clin. Pharmacol. *82*, 943–956.

44. Jiang, W., Cheng, Y., Zhao, N., Li, L., Shi, Y., Zong, A., and Wang, F. (2018). Sulfated polysaccharide of Sepiella Maindroni ink inhibits the migration, invasion and matrix metalloproteinase-2 expression through suppressing EGFR-mediated p38/MAPK and PI3K/Akt/mTOR signaling pathways in SKOV-3 cells. Int. J. Biol. Macromol. *107* (Pt A), 349–362.

45. Yang, F., Li, X., Yang, Y., Ayivi-Tosuh, S.M., Wang, F., Li, H., and Wang, G. (2019). A polysaccharide isolated from the fruits of Physalis alkekengi L. induces RAW264.7 macrophages activation via TLR2 and TLR4-mediated MAPK and NF-κB signaling pathways. Int. J. Biol. Macromol. *140*, 895–906.

46. Deng, C., Fu, H., Shang, J., Chen, J., and Xu, X. (2018). Dectin-1 mediates the immunoenhancement effect of the polysaccharide from Dictyophora indusiata. Int. J. Biol. Macromol. *109*, 369–374.

47. Zhang, X., Ding, R., Zhou, Y., Zhu, R., Liu, W., Jin, L., Yao, W., and Gao, X. (2013). Toll-like receptor 2 and Toll-like receptor 4-dependent activation of B cells by a polysaccharide from marine fungus Phoma herbarum YS4108. PLoS ONE *8*, e60781.

48. Li, R., Fang, L., Pu, Q., Bu, H., Zhu, P., Chen, Z., Yu, M., Li, X., Weiland, T., Bansal, A., et al. (2018). MEG3-4 is a miRNA decoy that regulates IL-1β abundance to initiate and then limit inflammation to prevent sepsis during lung infection. Sci. Signal. *11*, eaao2387.

49. Feng, S., Cong, S., Zhang, X., Bao, X., Wang, W., Li, H., Wang, Z., Wang, G., Xu, J., Du, B., et al. (2011). MicroRNA-192 targeting retinoblastoma 1 inhibits cell proliferation and induces cell apoptosis in lung cancer cells. Nucleic Acids Res. *39*, 6669–6678.

50. Sharma, K., Goehe, R.W., Di, X., Hicks, M.A., 2nd, Torti, S.V., Torti, F.M., Harada, H., and Gewirtz, D.A. (2014). A novel cytostatic form of autophagy in sensitization of non-small cell lung cancer cells to radiation by vitamin D and the vitamin D analog, EB 1089. Autophagy *10*, 2346–2361.

51. Li, R., Tan, S., Yu, M., Jundt, M.C., Zhang, S., and Wu, M. (2015). Annexin A2 Regulates Autophagy in Pseudomonas aeruginosa Infection through the Akt1-mTOR-ULK1/2 Signaling Pathway. J. Immunol. *195*, 3901–3911.

OMTO, Volume *20*

Supplemental Information

Therapeutic potential of IBP as an autophagy inducer for treating lung cancer via blocking PAK1/Akt/mTOR signaling

Huimin Bu, Shirui Tan, Bo Yuan, Xiaomei Huang, Jiebang Jiang, Yejiao Wu, Jihong Jiang, and Rongpeng Li

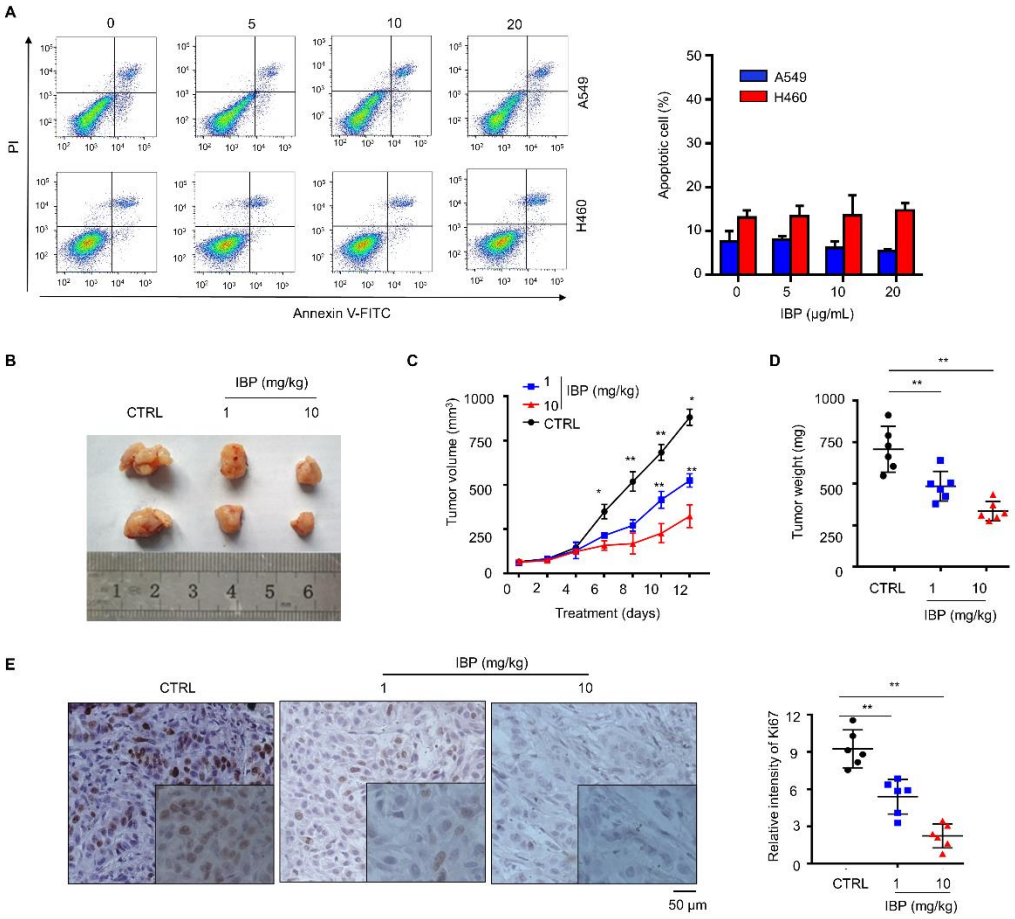

Figure S1. IBP inhibits lung cancer cells in an apoptosis-independent way. **(A)** A549 and H460 cells were incubated in the presence of IBP at different concentrations (0, 5, 10, 20 μg/mL) for 48 h. The apoptotic lung cancer cells was assessed by flow cytometry assay. **(B-D)** H460 cells were subcutaneously inoculated in the back of Balb/C mice. 1 or 10 mg/kg of IBP was administered by intraperitoneal injection every 2 days when the tumor was felt and the tumor size was measured. Mice were sacrificed on day 12, and tumors were excised, photographed and weighted. **(E)** Ki67 expression in tumor xenografts was examined by IHC. Representative images were provided as indicated; Scale bar, 50 mm. Data are mean ± SD from three independent experiments. One-way ANOVA (Tukey's post hoc); $*p < 0.05$; $**p < 0.01$.

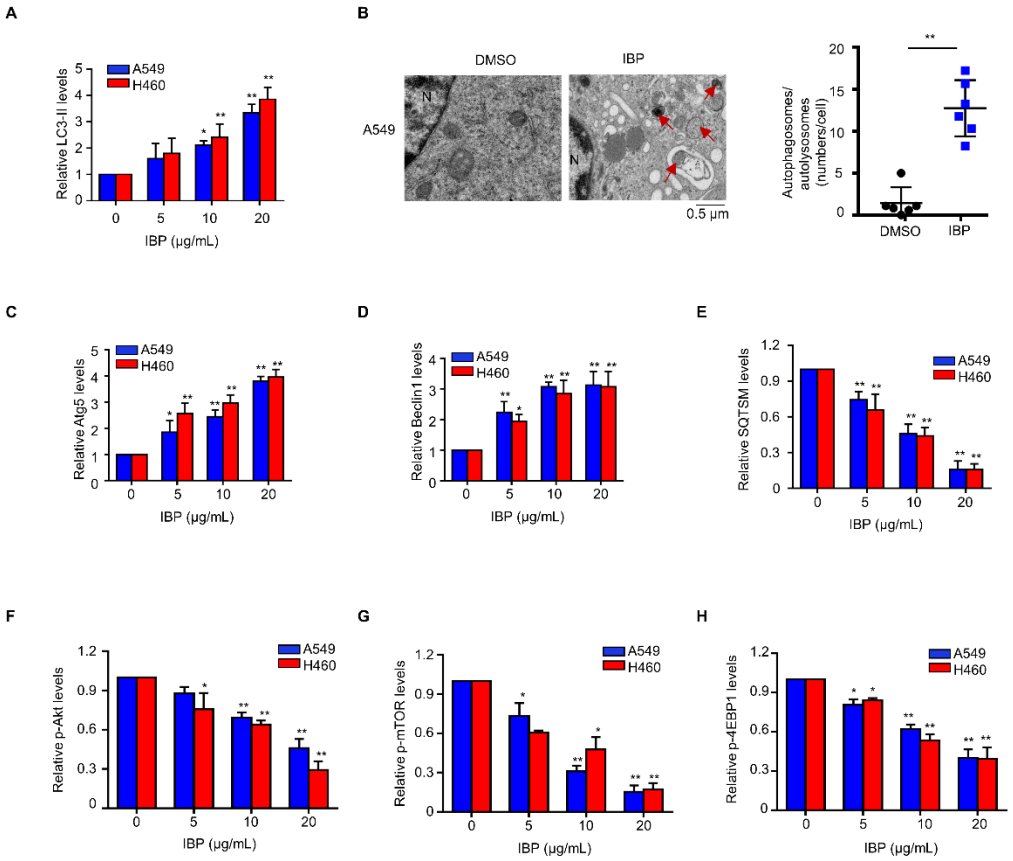

Figure S2. Densitometric quantification of the immunoblotting gel data presented in main Figures (in text) and autophagosome in A549 cells. (A) Fig. 2A, **(B)** Autophagy measured by transmission electron microscopy in A549 cells. Arrows, autophagosomes. Cells treated with DMSO or 10 μg/mL IBP for 48 hours was examined. **(C-E)** Fig. 2A. **(F-H)** Fig. 4D. Data are mean ± SD from three independent experiments. One-way ANOVA (Tukey's post hoc); *$p < 0.05$; **$p < 0.01$.

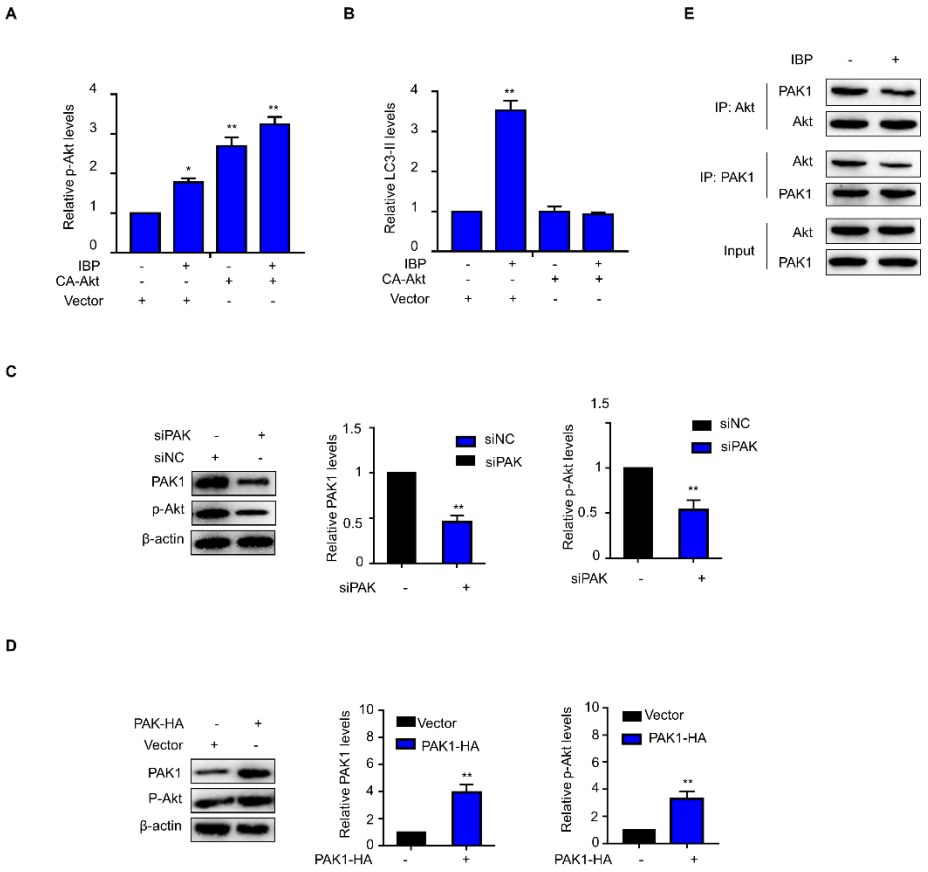

Figure S3. IBP inhibits Akt/mTOR pathway in A549 cells and Interaction of PAK1 with Akt in A549 cells. (A-B) Fig. 4E**. (C-D)** PAK1 levels and Akt phosphorylation in A549 by Western blot analysis. Cells were transfected with siPAK1 (C) or a construct encoding PAK1-HA (D) for 48 hours. **(E)** IP-western blots analysis of the interaction of PAK1 with Akt. A549 cells were treated with 10 μg/mL IBP or DMSO for 48 hours after cells were co-transfected with PAK1-HA and Akt-GFP. Data are a representation of 3 independent experiments. One-way ANOVA (Tukey's post hoc); *, p <0.05; **, p <0.01.

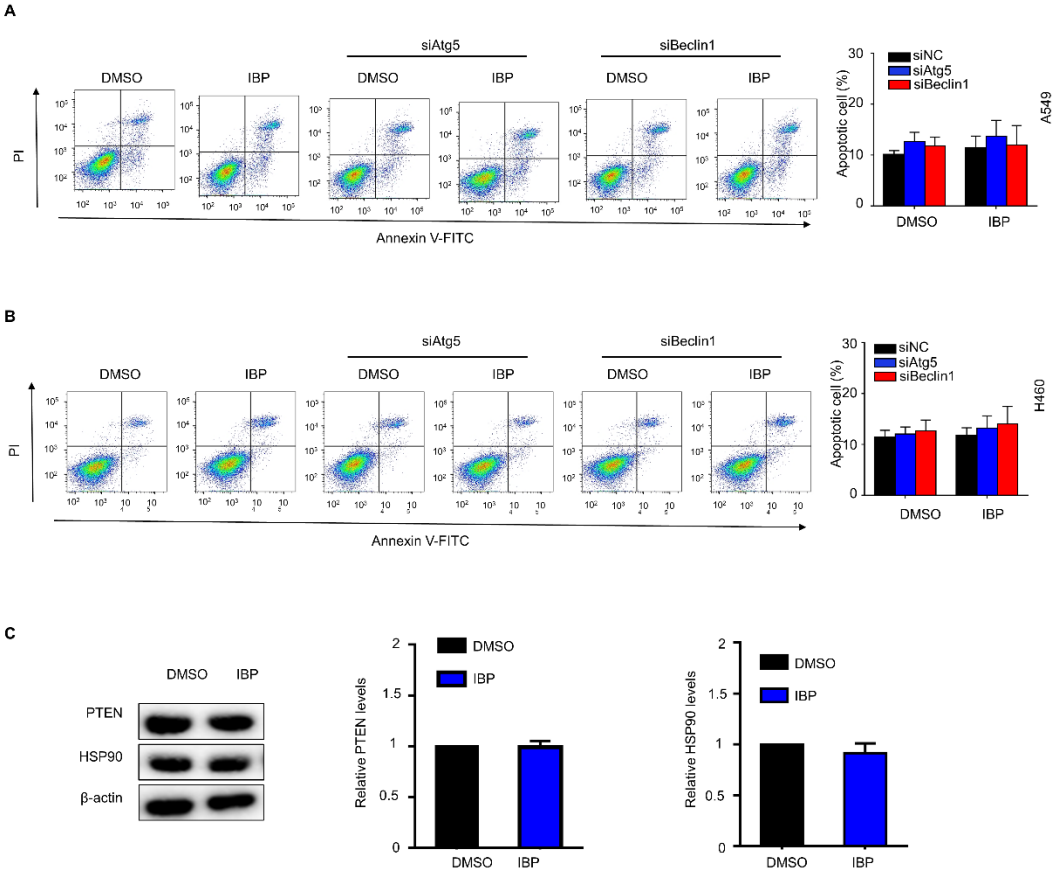

Figure S4. IBP treatment showed no obvious effect on apoptosis cells in an autophagy-independent way and PETN and HSP90 expression in A549**. (A-B))** A549 and H460 cells were transfected with siRNA against Atg5 or Beclin1 or control (50nmol/L) for 48 hours. Then cells were treated with 10 μg/mL IBP or DMSO for 48 hours. **(C)** PTEN and HSP90 in A549 by Western blot analysis. Data are shown as means ± SD for three independent experiments (cell samples, Tukey's post hoc; *$p \leq$ 0.05; **$p \leq 0.01$).